



Author: Scott J. Menegon, John L. Wilson, Nelson T. K. Lam, and Emad F. Gad
Title: Experimental assessment of the ultimate performance and lateral drift behaviour of precast concrete building cores
Year: 2020
Journal: Advances in Structural Engineering
URL: <http://hdl.handle.net/1959.3/455638>

Copyright: Copyright © 2020 the author(s). This version is licensed under a Creative Commons Attribution-NonCommercial-NoDerivatives 4.0 International License in compliance with publisher policy. See <https://creativecommons.org/licenses/by-nc-nd/4.0/>

This is the author's version of the work, posted here with the permission of the publisher for your personal use. No further distribution is permitted. You may also be able to access the published version from your library.

The definitive version is available at: <https://doi.org/10.1177/1369433220919077>

Experimental Assessment of the Ultimate Performance and Lateral Drift Behaviour of Precast Concrete Building Cores

Scott J. Menegon^{1,*}, John L. Wilson¹, Nelson T. K. Lam² and Emad F. Gad¹

¹ Department of Civil and Construction Engineering, Swinburne University of Technology, Melbourne, Australia.

² Department of Infrastructure Engineering, University of Melbourne, Melbourne, Australia

* Corresponding Author. Email: scott@menegon.com.au.

Abstract: Precast concrete building cores are a widely used lateral load resisting system in low and mid-rise multi-storey buildings. However, despite their widespread use in countries like Australia or New Zealand, very little research or experimental testing has been undertaken to assess their lateral drift behaviour. This paper will present the findings and observations of a recent experimental testing program into reinforced concrete (RC) precast building cores, which included three largescale 'box-shaped' precast building core specimens. Adjacent panels in each specimen were connected together using welded stitch plate (WSP) connections and then connected to foundation blocks on the top and bottom using grout tube connections. The results of the testing showed that the WSP connections were too flexible to allow full composite action to be developed in the cross-section, which meant the precast building core specimens were around 25% more flexible than an equivalent cast in-situ version. The testing also highlighted common detailing and construction deficiencies that can severely inhibit the ductility of the core.

Keywords: RC walls; RC building cores; precast construction; Precast cores.

1 Research Significance and Background

Over the last 10 to 20 years precast concrete walls and building cores have become increasingly popular options for the primary lateral load resisting system in low and mid-rise buildings in regions of lower seismicity, such as Australia (Menegon et al., 2017c), as well as in some regions of higher seismicity, such as New Zealand (Seifi et al., 2016). Precast construction offers many benefits over traditional cast in-situ RC construction, which includes more efficient and faster on-site construction

timeframes and high-quality construction tolerances that can be achieved in an off-site warehouse manufacturing environment.

Various research studies have been undertaken to develop new innovative precast wall systems (e.g. Sun et al. (2015); Sun et al. (2018); Jiang et al. (2019)), however limited investigations have been performed to assess the types of precast wall systems that have been widely adopted and used in Australia for many years, as identified by Menegon et al. (2017c). Similar systems are also used in other regions of lower seismicity abroad. The performance of these systems has typically been assessed and determined using theoretical approaches in structural engineering design offices. Some limited experimental studies have been performed to assess the in-plane drift behaviour of isolated rectangular walls panels (e.g. (Seifi et al., 2019)), however even less research attention has been given to precast building core systems, which is the primary focus of this study.

Precast building core systems, typical of low seismic regions like Australia, generally consist of four individual rectangular RC panels that are cast off-site and later transported to and erected on-site to form a box-shaped building core. The panels are connected vertically to panels above/below using grout tube connections and horizontally to adjacent panels using welded stitch plate (WSP) connections. The WSP connections allow vertical shear forces to be transferred between adjacent panels, which allows the individual panels to act together as one composite cross-section.

This paper presents the findings and observations of a recent large-scale experimental testing program into limited ductile reinforced concrete (RC) precast building cores. The primary objective was to assess the in-plane lateral drift behaviour and ductility of these systems, particularly with reference to the post-yield and post-peak non-linear response. The specimens were constructed to best match industry standard construction in Australia, as identified in Menegon et al. (2017c).

This meant the specimens were designed and detailed to be 'limited ductile' elements in accordance with the 2009 Australian standard for concrete structures, AS 3600 (Standards Australia, 2009). The limited ductile classification allows the designers to calculate pseudo equivalent static earthquake forces in accordance with AS 1170.4 (Standards Australia, 2007) using a force reduction factor of 2.6 (i.e. ductility factor 2.0 and an overstrength factor of 1.3).

Despite the lower seismic nature of Australia, due to it being an intraplate region, earthquake actions are typically the critical lateral design case for many buildings that utilise these systems. Regardless of this, and the somewhat generous force reduction factors adopted when calculating the seismic design loads, these systems are typically designed without any consideration of ductility, capacity design principles or designation of an appropriate energy dissipating system. An objective of this study is to experimentally assess the appropriateness of these precast systems for the ductility assumptions widely assumed in industry for buildings of this nature.

2 Experimental Work

2.1 Test Program

The experimental system level precast building core testing program consisted of three specimens denoted S03, S04 and S05. The three specimens were constructed to generally match the geometry (i.e. height and wall length) of a cast in-situ building core specimen previously tested by the authors, denoted S02 (Menegon, 2018; Menegon et al., 2017b).

The specimens were designed and tested to represent the ground floor component of a taller four-storey building core (refer Fig. 1). This style of test setup, often referred to as ‘panel testing’, allows for walls to be tested with high shear-span ratios that would otherwise be logistically difficult and too large for the majority of test laboratories, and has become a widely used testing procedure for RC walls in recent years (e.g. Lowes et al. (2012); Almeida et al. (2017); Dashti et al. (2017); Lu et al. (2017); Segura and Wallace (2018); Shegay et al. (2018)). Under this test setup, an in-plane lateral moment, coupled to the lateral force of the specimen, is applied to simulate the bending moment and shear force response of the taller four storey wall. The applied moment in this test program was equal to the in-plane force multiplied by a value of 5.2, which results in the equivalent response of four-storey wall subject to an inverted triangular load distribution, or more simply, a wall tested with a shear-span ratio of 6.5.

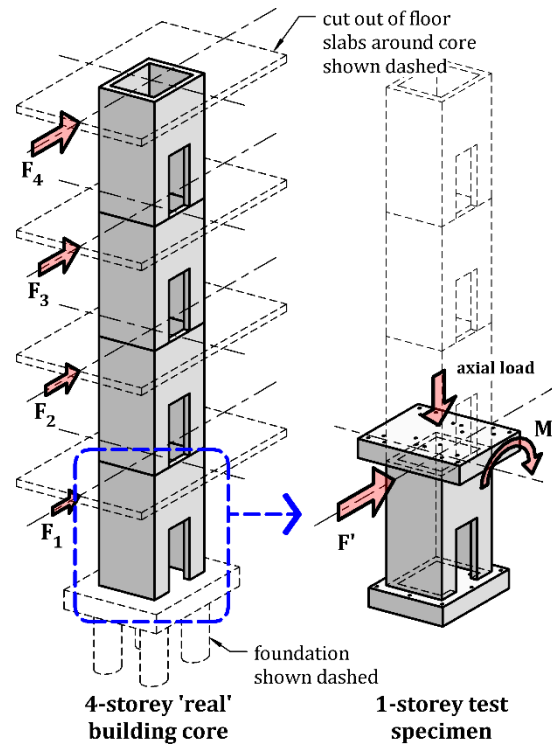


Fig. 1. Simulation of a four-storey building response using a one-storey test specimen.

2.2 Test Specimen Overview

The three specimens had a height of about 2600 mm, width of 1200 mm and length of 1200 mm. The panel thickness of S03 and S04 was 130 mm and for S05 it was 150 mm. The overall geometry, cross-sections and WSP connections for each specimen are shown in Fig. 2. The precast panels for all three specimens were manufactured by a local precast manufacturer in Melbourne. Specimens S03 and S04 were assembled by the manufacturer, whereas the panels for specimen S05 were delivered to the Smart Structures Laboratory (SSL) at Swinburne and the building core was assembled on site.

The geometry of the test specimens was constrained by the test machine and as such they were designed to represent a 60–70% scaled ground storey building core in a real building with dimensions as follows: height of 4000 mm; width and length of 2000 mm; and wall thickness of 200 mm.

The panels were constructed using a standard N40 grade concrete mix, which has a minimum characteristic 28-day compressive cylinder strength of 40 MPa. The panels for each specimen were cast on different days, resulting in the actual concrete strengths for the individual panels in each specimen being different. The actual concrete strength on test day for specimens S03, S04 and S05 ranged from 40.7–47.9, 43.5–45.47 and 35.2–44.5 MPa respectively.

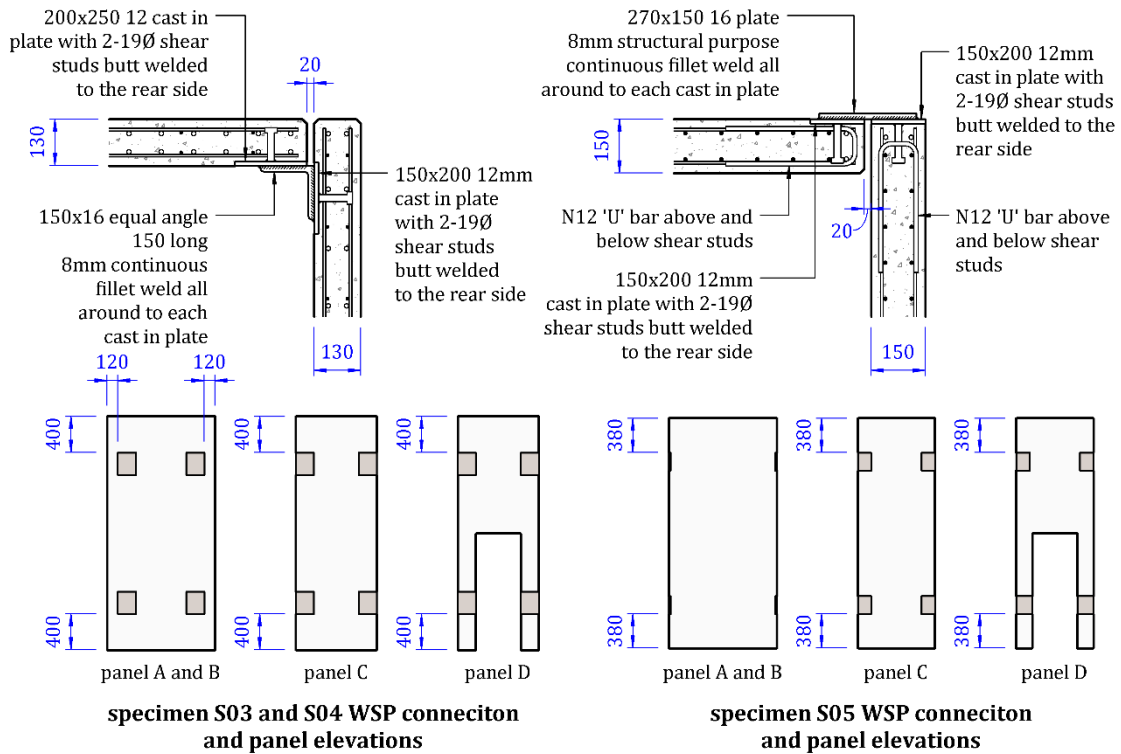
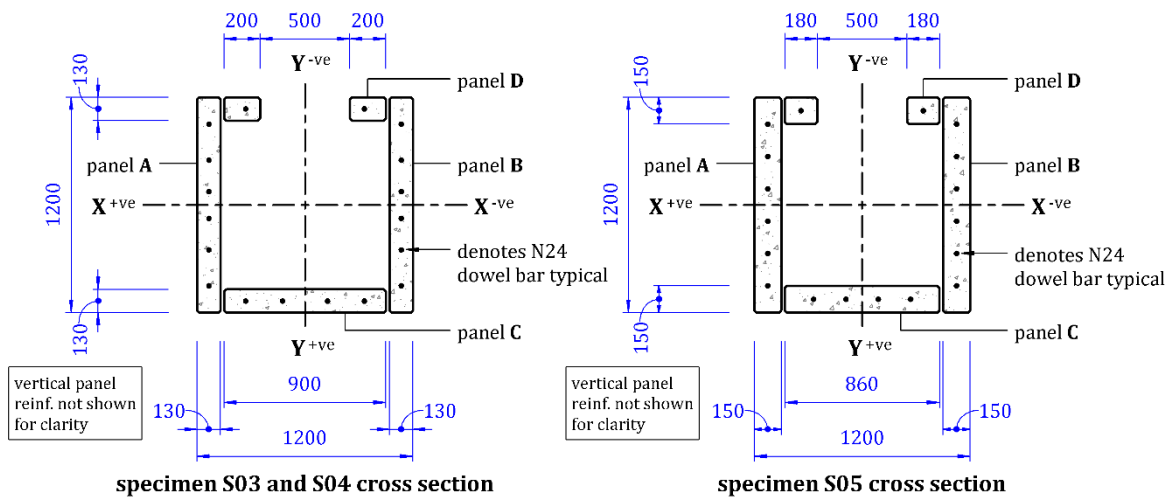
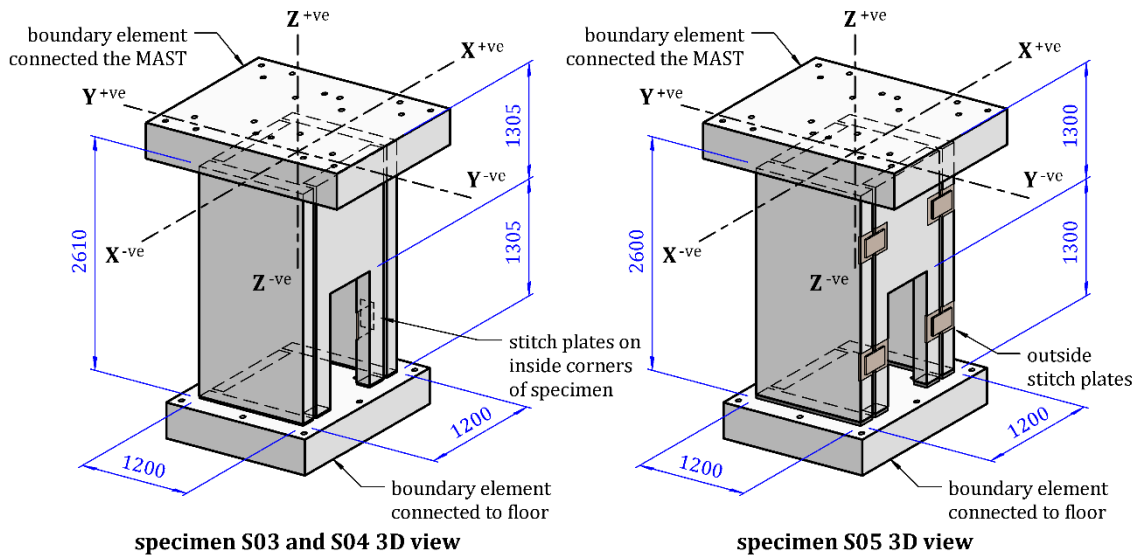


Fig. 2. Perspective views of test specimens S03 to S05.

The concrete strength of each panel was determined from 100 mm diameter and 200 mm high concrete cylinder samples that were cast with each respective panel and cured in a similar environment. The concrete strengths for each individual panel, in each specimen, are summarised and presented in Menegon (2018).

The specimens were constructed using WSP connections that were representative of 'industry standard' connections in Australia (Menegon et al., 2017c). The WSP connections have steel plates, with shear studs welded to the rear side, cast into the edges of adjacent RC panels. After the panels are erected in place, a third steel plate is site welded to each adjacent cast in plate. This connection also allows a generous amount of construction tolerance so the panels can be easily and accurately aligned into their required position. WSP connections of this nature typically result in a 20 mm vertical gap between adjacent panels. A backing rod and strip of fire rated sealant is typically then installed vertically along/between this 20 mm gap.

Specimens S03 and S04 were constructed with 'inside fixed' stitch plates, where the connection is located on the inside of the core, whereas S05 was constructed using an 'outside fixed' stitch plate, where the connection is located on the outside of the core. Each of these connections are shown in Fig. 2. Additionally, panel elevations showing the location of the cast-in plates for each specimen are also provided in Fig. 2. Material samples of the structural steel plates for the stitch plate connections were not taken, however the steel plates and welds did not undergo any inelastic behaviour during the testing, maintaining an elastic response.

Similar to the WSP connections, the specimens were constructed using industry standard grout tube connections that have corrugated metal grout tubes cast vertically into the base of the panel that slots over a starter bar (or dowel bar) from the foundation under. The grout tube is typically at least twice the diameter of the dowel bar, allowing for a generous amount of construction tolerance so the panels can be easily erected and accurately aligned. There are no specific 'code requirements' for a minimum/maximum grout tube diameter, and the diameter is selected based on desired construction tolerances. After the panels are erected, the base of the panel is 'dry packed' with a cementitious grout and the grout tube is then filled the next day using a flowable high strength cementitious grout, which then creates an integral connection between the base of the panel and the surrounding RC structure. Typical industry practice in Australia is to 'gravity pour' the grout tubes using a flowable grout mix.

Despite the relative high construction standards in Australia and the functional importance these connections have to the final in-situ performance of the structure, this process is generally an unregulated and unchecked activity on site. Thus, resulting in little assurance that the tubes are completely filled without voids. This is in sharp contrast to New Zealand, where the grout tubes are usually pumped from an outlet at the base until they overflow from an outlet at the top of the tube, thereby ensuring the grout tubes are filled properly. The latter is clearly a superior approach and would be recommended for adoption in Australia.

The panels in the specimens were connected to the top and bottom boundary elements using the grout tube connection shown in Fig. 3. This consisted of 50 mm diameter corrugated grout tube, which was filled using Aitken Freemans Tecgrout HS that has a 90 MPa characteristic compressive strength at 28 days. The grout was mixed using the higher water content required to achieve a flowable mix – such that gravity pouring of the grout tubes could be achieved without any air pockets forming – which meant the strength of the grout was lower than the characteristic strength. The grout strength varied between 67 and 78 MPa on test day. The grout strength was determined using 50 mm cube samples. This meant the grout strength was about 20 to 30 MPa stronger than the panels.

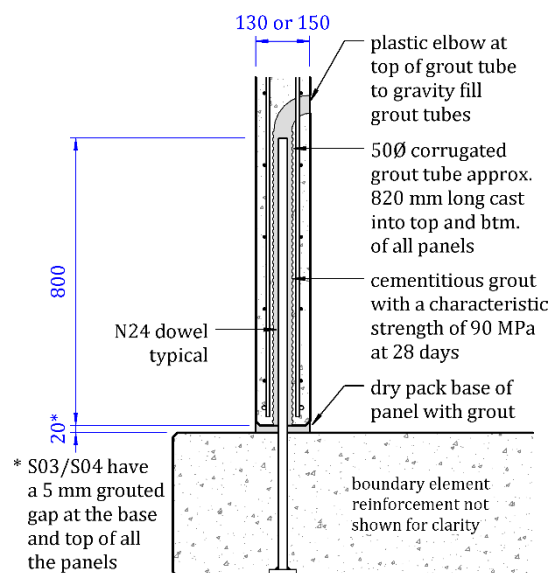


Fig. 3. Panel to foundation block grout tube connection.

There is no specific codified approach in the Australia standard for concrete structures, AS 3600 (Standards Australia, 2009), which the specimens were designed and detailed in accordance with, for calculating the embedment length of dowel bars in grout tubes; the embedment length is usually just

calculated based on the development rules for normal rebar in concrete. This approach was used for the specimens and a subsequent embedment length of 800 mm was used.

The panels were constructed using D500N or D500L reinforcement in accordance with AS/NZS 4671 (Standards Australia and Standards New Zealand, 2001). D500N and D500L denotes deformed (i.e. ribbed) normal and low ductility reinforcement respectively, with a minimal characteristic yield stress 500 MPa. The minimum characteristic strain hardening ratios are 1.08 and 1.03 respectively and the minimum characteristic uniform elongations are 5% and 1.5% respectively.

The reinforcement for each panel generally consisted of a sheet of low ductility (i.e. D500L) welded mesh on each face of the panel with additional normal ductility (i.e. D500N) vertical bars at each end. Some panels then had additional D500N vertical bars intermediately across the length of the panel. The vertical reinforcement in each panel of each specimen is summarised in Table 1, where N12 denotes a 12 mm nominal diameter reinforcing bar that is grade D500N and similarly, L7.6 denotes a 7.6 mm nominal diameter reinforcing bar that is grade D500L. Panel references for each specimen are provided in Fig. 2. The panel with the opening in it (i.e. Panel D), had 4-N12 in the panel legs either side of the opening, for all specimens. No additional D500N horizontal bars were used in the specimens, so the horizontal reinforcement in the panels consisted of just the welded mesh. This generally meant the panels had L7.6 bars at 200 mm centres on each face, except for Panel B in S03, which had L8.6 bars at 200 mm centres on each face.

Table 1. Vertical reinforcement in each panel for test specimens S03 to S05.

Specimen	Vertical reinforcement per face			Vertical reinforcement ratio		
	Panel A	Panel B	Panel C	Panel A	Panel B	Panel C
S03	8-N12 and 6-L7.6	10-N12 and 6-L8.6	10-N12 and 4-L7.6	0.015	0.019	0.022
S04	12-N12 and 11-L10.7	12-N12 and 11-L10.7	8-N12 and 9-L10.7	0.030	0.030	0.029
S05	2-N12 and 11-L9.5	2-N12 and 11-L9.5	2-N12 and 8-L9.5	0.011	0.011	0.012

Each panel typical had 6-N24 dowel bars at the top and bottom of the flange panels (i.e. Panels A and B) and 4-N24 dowel bars in the web panels (i.e. Panel C). The panel with the opening in it (i.e. Panel D), had 1-N24 in the panel legs either side of the opening. The dowel bar reinforcement in each panel of each specimen is summarised in Table 2. Further information regarding the reinforcement

detailing, construction details/drawings of the specimens and the actual reinforcement material properties determined from tensile tests of material samples are provided in Menegon (2018).

Table 2. Dowel bar size in each panel for test specimens S03 to S05.

Specimen	Dowel reinforcement			Dowel reinforcement ratio		
	Panel A	Panel B	Panel C	Panel A	Panel B	Panel C
S03	6-N24	6-N24	4-N24	0.017*	0.017*	0.015 [†]
S04	6-N24	6-N24	4-N24	0.017*	0.017*	0.015
S05	6-N24	6-N24	4-N24	0.015	0.015	0.014

* The dowel reinforcement ratio for panels A and B of specimens S03 and S04 was effectively decreased to 0.012 because two of the N24 dowel bars in each panel needed to be relocated and when the new bars were epoxied into the boundary element block, they were not epoxied correctly, allowing them to prematurely to pull-out and failure relatively early in the test.

[†] Similar to panels A and B as discussed above, the dowel bar at the positive x-axis end of panel C in specimen S03 prematurely failed also, meaning the reinforcement ratio was effectively decreased to 0.011 in panel C.

Due to some construction errors, specimens S03 and S04 ended up varying slightly from what was originally intended. These errors resulted in S03 having an unsymmetrical reinforcement layout (as highlighted in Table 1) and some of the dowel bars in the bottom boundary element of specimens S03 and S04 being cast in the wrong location. As a result, these dowel bars had to be cut off so new bars could be epoxied into the bottom boundary element in the correct locations. However, the new relocated bars were not epoxied as specified and, during testing of the specimen, pull out failure of the bars – due to bond failure of the epoxy – occurred relatively early when a low amount of lateral displacement was being applied. Specimens S03 and S04 were meant to represent the scenario where a precast wall is designed to have equal dowel bar reinforcement to wall panel reinforcement, which results in the inelastic strains and curvatures being shared between cross-section of wall at the joint itself and the cross-section of wall above the joint. However, these construction errors meant that S03 and S04 now represent an alternative design scenario, which is commonly seen in industry, where precast panels are detailed with significantly less dowel bar reinforcement relative to the panel reinforcement over. Under this scenario, the inelastic strains and curvatures are usually then concentrated at the very base of the wall and within the cross-section of wall located at the grout tube connection. This then results in the formation of one large crack and a concentration of inelastic strains and curvatures at this single crack location.

2.3 Test Setup and Loading Protocol

The specimens were tested using the Multi-Axis Substructure Testing (MAST) System in the Smart Structures Laboratory (SSL) at Swinburne University of Technology. The MAST System is a state-of-the-art test machine capable of applying full six degree-of-freedom (DOF) loading in mixed-mode, switch-mode, hybrid or combination therein (Hashemi et al., 2015). The detailed specifics of the MAST System (including actuator layouts and capacities) are presented in Menegon (2018).

The specimens were tested under unidirectional quasi-static cyclic test conditions. Initially an axial load was applied to the test specimens to simulate the pre-compression load on the wall (i.e. the gravity load from the surrounding building). The applied axial load for all specimens was -1200 kN. It was applied in force-controlled mode in the z-axis (T_z) and maintained for the duration of the test. This resulted in axial load ratio (i.e. axial load divided by the product of the gross cross-sectional area of wall and the compressive strength of the concrete) of approximately 5.6%, 5.7% and 5.3% for specimens S03, S04 and S05 respectively.

After the axial load was applied to the specimens, the specimens were subject to incrementally increasing cyclic lateral displacements in the x-axis (T_x). For each lateral displacement increment the specimens were subjected to two positive and two negative cycles, in line with the recommendations given in ACI 374.2R-13 (American Concrete Institute, 2013). The displacement increments adopted for the test were the same values the authors used to test the cast in-situ equivalent building core specimen presented in Menegon et al. (2017b); wherein displacement increments were selected so subsequent values were between 5/4 and 3/2 times the current value. This procedure for calculating subsequent lateral displacement increments was determined with reference to ACI ITG-5.1-07 (American Concrete Institute, 2008). This resulted in loading series with commanded lateral displacements corresponding to the following lateral drifts: series 1, $\pm 0.2\%$; series 2, $\pm 0.3\%$; series 3, $\pm 0.4\%$; series 4, $\pm 0.5\%$; series 5, $\pm 0.8\%$; series 6, $\pm 1.1\%$; series 7, $\pm 1.5\%$; series 8, $\pm 1.9\%$; series 9, $\pm 2.7\%$; series 10, $\pm 3.8\%$; and series 11, $\pm 5.4\%$. It should be noted the actual specimen drifts calculated using independently mounted instrumentation varied from the commanded machine drifts stated above. The results and discussion hereafter will use the actual drift values for each respective specimen, rather than these commanded machine values. The loading rate varied such that it took approximately 60 seconds to reach each displacement increment. The test was paused at the second

positive and second negative cycle of each increment to take photos, mark cracks and take photogrammetry measurements.

For the duration of the test a moment was applied about the y-axis in force-controlled behaviour (as discussed previously, refer Fig. 1) and was equal to the in-plane x-axis force multiplied by a value of 5.2. This results in the specimens having a shear-span ratio of 6.5. The remaining out-of-plane DOFs were commanded to zero displacement and zero rotation in displacement-controlled behaviour for the duration of the test. The x-y-z loading axes for the specimens are shown in Fig. 2.

An important aspect of the test setup to note is that the top boundary element of each specimen (refer Fig. 2) will provide additional restraint between adjacent panels, which will limit the amount of vertical movement between the panels. Essentially this will create additional 'coupling' behaviour between adjacent panels and allow better composite action to be developed in the core than would otherwise be developed if there were just WSP connections alone connecting the panels. This behaviour however, is not necessarily unrealistic or unrepresentative of the behaviour that would be seen in a real building. Many RC wall buildings that utilise precast walls/cores have 200 to 300 mm thick cast in-situ flat slab floor plates. The flat slabs are usually either poured 'over the top' of the wall with vertical dowels running through the slab to the panel above or 'hard up against' the side of the panels with a 30 mm (give or take) shear key recessed into the face of the panel, with additional drag bars from the panel that are cast into the slab. The floor slab in this scenario will provide some additional coupling behaviour between adjacent panels, similar to the top boundary element in these test specimens.

3 Results and Discussion

This section will outline the test results for specimens S03, S04 and S05. The general in-plane lateral performance of all three specimens will be discussed initially, followed by an in-depth analysis of the results where the focus is generally with respect to S05. The latter will discuss the following in six separate sub-sections: crack propagation and curvature distribution; WSP connection performance; equivalent single DOF response and effective stiffness; displacement ductility and overstrength; deformation components, i.e. flexure, shear and sliding shear; and overall composite behaviour.

3.1 General Specimen Response

The force-displacement behaviour for specimens S03, S04 and S05, at the top of the specimens, are presented in Fig. 4. These plots only show the specimen response up until significant strength degradation occurred (i.e. the lateral strength dropped below 50% of the maximum lateral strength), for clarity. The specimens were subjected to larger in-plane lateral drifts than shown in these figures to better understand when and how complete structural failure occurs, i.e. when the element can no longer hold the initial axial load. Photos showing the condition of the specimens at the peak positive and negative strengths are presented in Fig. 5. The positive and negative strength of S03 was unsymmetrical (as shown in Fig. 4) because of the unsymmetrical reinforcement layout and the premature dowel bar failure at one end of the web panel, as discussed in the previous section.

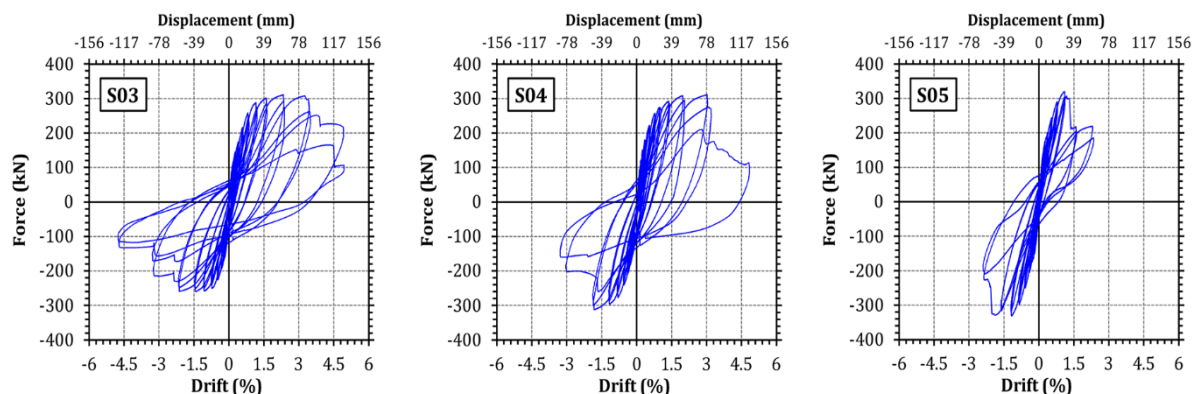


Fig. 4. Force-displacement response of specimens.

Varying levels of performance was observed in the three test specimens. Lateral load failure, which was defined to be when the lateral strength degraded below 80% of the maximum, occurred after lateral drift cycles of +2.4%/-2.1%, +3.0%/-1.9% and +1.1%/-1.2% were exceeded in specimens S03, S04 and S05 respectively.

Overall failure, which was defined to be when the lateral strength degraded to zero (while maintaining the initial axial load), occurred after lateral drift cycles +4.6%/-4.8%, +8.2%/-8.0% and +3.5%/-3.4% for test specimens S03, S04 and S05 respectively. It is noted that the positive lateral drift values are slightly larger than the negative lateral drift values and is due to the lateral displacement being commanded in the MAST System using the absolute x-axis displacement of the crosshead (i.e. the 'machine' displacement), as opposed to 'true' (i.e. relative) displacement of the specimen, which was obtained from independently mounted instrumentation.

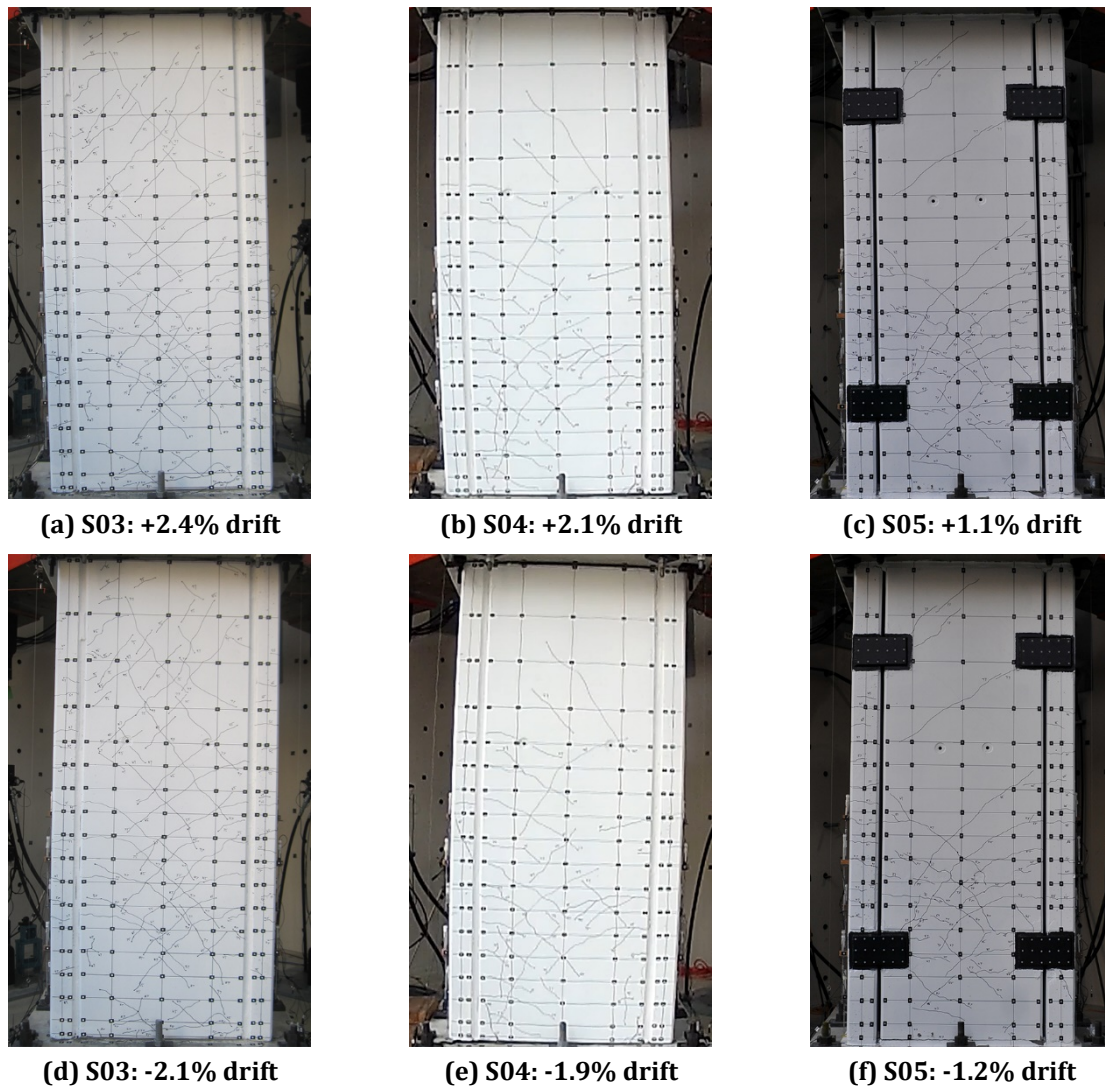


Fig. 5. Force-displacement response of specimens.

Axial load failure of the specimens, i.e. complete structural collapse, did not occur in any of the specimens. Specimens S03, S04 and S05 were subjected to +7.1%/-6.5%, +8.2%/-8.0% and +4.9%/-4.8% respectively and were all able to withstand the initial axial of -1200 kN. The test was terminated after each of these respective drift cycles. This further shows that RC elements with low axial load ratios – in this case, varying between 5.2–6.3% – can withstand significant in-plane lateral drifts before complete structural collapse, which was highlighted in a recent study on RC columns by Wilson et al. (2015).

All three specimens had force-displacement hysteresis curves that were not overly ‘stable’ and were subjected to various premature failure mechanisms (refer Fig. 4), which could have potentially been avoided through good reinforcement detailing. Specimens S03 and S04 (due to the construction problems discussion earlier), had a weak section at the base of the of wall due to the percentage of

dowel bar reinforcement being relatively much smaller than the vertical reinforcement in the panels. This meant that all the inelastic/plastic behaviour was concentrated at the base of wall in one location – similar to what is seen in lightly reinforcement cast in-situ walls (e.g. Lu et al. (2017) and Lu and Henry (2017)) – allowing very large tensile strains to be developed in the dowel bars. This resulted in the first dowel bar fracturing in specimen S03 at approximately -2.4% lateral drift. If the area of dowel reinforcement was higher than the vertical reinforcement in the panel, the plastic behaviour could have potentially been distributed over many cracks that would then result in smaller tension strains in the dowels for the corresponding displacement increment, which would then result in an increased displacement capacity of the core. Similarly, the first dowels fractured in S04 at around -1.6% drift while the specimen was being loaded to the first -3% drift load cycle. The lateral capacity in S04 then subsequently dropped to about 65% of its maximum.

This curvature distribution seen in S03 and S04 – where all the plastic strains are concentrated at the base of the wall across one large crack – essentially allowed for a rocking mechanism to develop, which then allowed for very large lateral drifts without axial load failure of the building core occurring. Building core sections tend to have very high neutral axes (i.e. the neutral axis is close to the extreme compressive fibre) due to the very large compression flange of the section. This meant at the base of the specimen the compression flange was in compression, the tension flange was in tension and the majority of the web was then also in tension. This mechanism, with very high plastic tension strains in the dowels and effectively only one face of the core in compression, would result in a weak region at the base of the wall that would likely have little resistance to torsional actions. Torsional actions are common design actions for building cores in multi-storey buildings and therefore this rocking mechanism could likely result in sudden failures if being unexpectedly subject to torsional actions (which could be generated mid-way through a buildings response to ground shaking as elements yield and the load is redistributed throughout the structure). As such, it is being recommended in design to ensure the dowel bar area is greater than the area of vertical panel reinforcement to prevent large concentrated regions of inelastic strains developing.

Specimen S05 failed via fracturing of the vertical reinforcement at the first crack above the grout tube connection on the first positive load cycle that exceeded 1.1% lateral drift. Bar fracture at such a small amount of drift was caused by the panels being predominantly detailed using low ductile

reinforcement (i.e. D500L mesh), which is common practice for precast RC wall panels in Australia. The majority of the plastic strains were concentrated in one crack, despite multiple cracks initially developing, due to the low strain hardening ratio of the D500L mesh.

The lateral strength of S05 dropped to about 70% of the maximum after fracturing of the mesh in the flange panels, but then was maintained at this level because of the contribution from the two normal ductility bars at each end of the flange panels (i.e. the 2-N12 perimeters bar) and the mesh in the web panel of the specimen (as only the mesh in the flange panel fractured). A very wide crack was subsequently developed at this location. This would then likely result in this section of the core having little torsional resistance, for the same reasons hypothesised for the base region of S03 and S04. Furthermore, strength degradation between loading cycles of the same lateral drift increment increased significantly after the fracturing of the mesh.

Specimens S03 and S04 had poor horizontal grout interfaces at the base of panels compared to S05, which had a well grouted interface. This poor grout interface meant stress concentrations were able to develop in localised regions at the base of the compression flange panel, which resulted in premature compression failures due to vertical tensile splitting. This behaviour was observed in both S03 and S04; however, in S05, which had comparatively much better grouting, this behaviour was not observed. It is anticipated that nominal cross ties at the base of the panel would prevent this type of failure mode.

The grouting procedure, despite it being of critical importance to precast wall systems, is often an under-supervised activity on construction sites. As such, and unsurprisingly, instances of poorly grouted panel connections have been reported a number of times on building projects in Australia. Therefore, the authors recommend cross ties are always specified at the base of panels, even in non-ductile detailed wall systems, to prevent the likelihood of a tensile splitting failure mechanism developing.

Specimens S03, S04 and S05 generally all experienced low amounts of strength degradation between the first and second loading cycle for each respective displacement increment. However, significant strength degradation between loading cycles started to only after lateral load failure of the specimen had occurred (i.e. the lateral strength had degraded below 80% of the maximum lateral strength). Otherwise, the strength degradation between loading cycles was typically less than about 15%.

3.2 Crack Propagation and Curvature Distribution

Specimens S03, S04 and S05 were all detailed using moderate to high percentages of vertical reinforcement, meaning well distributed closely spaced cracking was expected and subsequently observed during the testing. Crack map summaries for each specimen are presented in Menegon (2018). In specimen S05, where the dowel bar reinforcement was better matched with the area of vertical reinforcement in the panels over, the plastic curvature distribution was across multiple cracks across the height of the specimen, as shown in Fig. 6. The curvature distributions were calculated using the contactless photogrammetry system. Tension face and compression face strains distributions, which was used to calculate the curvature distributions, are also presented in Menegon (2018).

The dowel connection at the base of the wall essentially created a localised region of overstrength, where the section was effectively reinforced with ~ 2 times the amount of vertical reinforcement as the section immediately below (that was reinforced by the dowel bars) and immediately above (that was reinforced by the vertical bars in the panel). This localised region of overstrength meant that the plastic curvature was concentrated at the base of the wall and directly above the dowel connection. A similar inelastic response was observed in the cast in-situ equivalent specimen, which had a lap splice of the vertical reinforcement at the base of the specimen (i.e. S02, refer Menegon et al. (2017b)) and was being referred to as a two-crack plastic hinge mechanism.

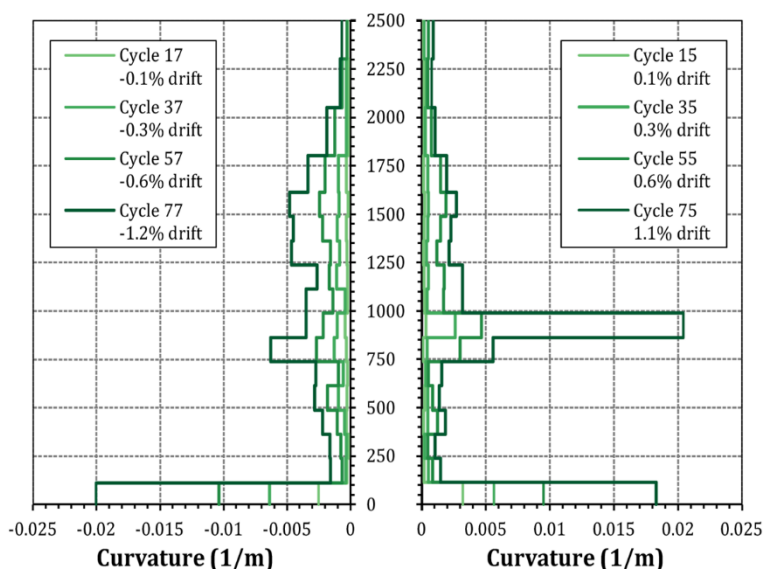


Fig. 6. Specimen S05 curvature distribution.

Interestingly, the inelastic plastic strains in the positive loading directions were predominantly concentrated in two cracks; the first at the base of the wall and second at the top of the dowel connection. Whereas in the negative loading direction, the inelastic plastic strains were concentrated between a single crack at the base of the wall and over multiple cracks directly above the dowel connection. The differing behaviour is expected to be a result of the low ductility vertical reinforcement, which has a very small strain hardening ratio and therefore limits the reinforcements ability to distribute inelastic strains, resulting in somewhat randomised strain localisations.

3.3 Stitch Plate Performance

The behaviour of the welded stitch plate (WSP) connections in specimen S05 were assessed using the contactless photogrammetry system and additional component level experimental testing performed by the authors (Menegon et al., 2017a; Menegon, 2018). In this testing an identical WSP connection to that used in S05 was tested until failure. This allowed a backbone curve of the WSP connections vertical shear force vs. differential vertical panel displacement to be determined. The force transferred through each stitch plate in S05 was then approximated by using the differential movement between panels (determined using photogrammetry markers above and below each stitch plate connection) and this backbone response of the isolated WSP connection. This process has been illustrated in Fig. 7 for the rear-face web panel WSP connections, which shows the approximated forces carried by each WSP connection for load cycles 15/17, 35/37, 55/57 and 75/77, which correspond to lateral drift values of +0.1%/-0.1%, +0.3%/-0.3%, +0.6%/-0.6% and +1.1%/-1.2% respectively.

It is shown in Fig. 7 that the maximum capacity of the rear-face WSP connections was not exceeded during load cycle 75 and 77, which corresponds to a lateral drifts of +1.1% and -1.2% respectively and the maximum capacity of the specimen being reached (refer Fig. 4). Although it should be noted that the force in the bottom WSP connection on the tension face of the specimen (i.e. stitch plate #3 during load cycle 77 and stitch plate #4 during load cycle 75) was only marginally less than the maximum 88 kN capacity of the connection. The front-face WSP connections (i.e. the face of the specimen with the opening) typically had smaller connection forces than the respective WSP connection in the corresponding location on the rear-face. The response/data for the four front-face WSP connections can be found in Menegon (2018).

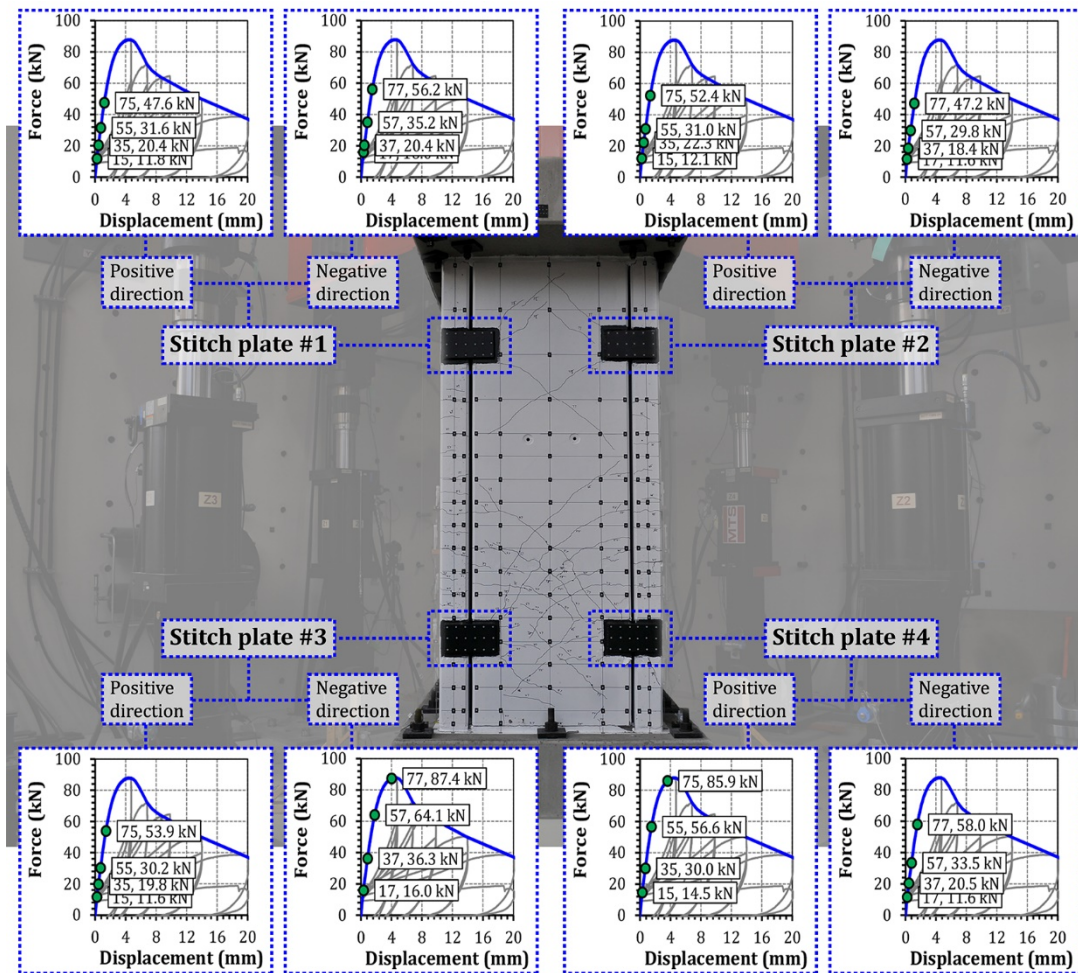


Fig. 7. Specimen S05 stitch plate performance using the component level test results.

3.4 Equivalent Single DOF Response and Effective Stiffness

The specimens represent the ground storey component of a taller four-storey building core, subjected to an inverted triangular lateral load distribution. This loading configuration is the equivalent of a three-storey wall subject to a single point load at the top. Therefore, the equivalent single degree-of-freedom response (or simply 1-DOF response) of the test specimens in this study, which have a shear-span ratio of 6.5 and a length of 1.2 m, would be the force-displacement behaviour of the three-storey building core shown in Fig. 8.

When assessing the performance of an RC wall or building core (e.g. effective stiffness, displacement ductility or unpacking the different components of deformations), the equivalent 1-DOF response should be used, otherwise misleading results or outcomes could be reported. This was demonstrated in Menegon (2018) where it was shown that the cast in-situ equivalent RC building core specimen mentioned previously (i.e. S02) had a percentage of flexural deformation of around 70%, when calculated based on the displacement results of only the test specimen itself. However, when the

equivalent 1-DOF response was determined and the percentage of flexural deformation was calculated using the 1-DOF displacement response results, the flexural percentage increased to about 90%, which is nearly a 30% increase.

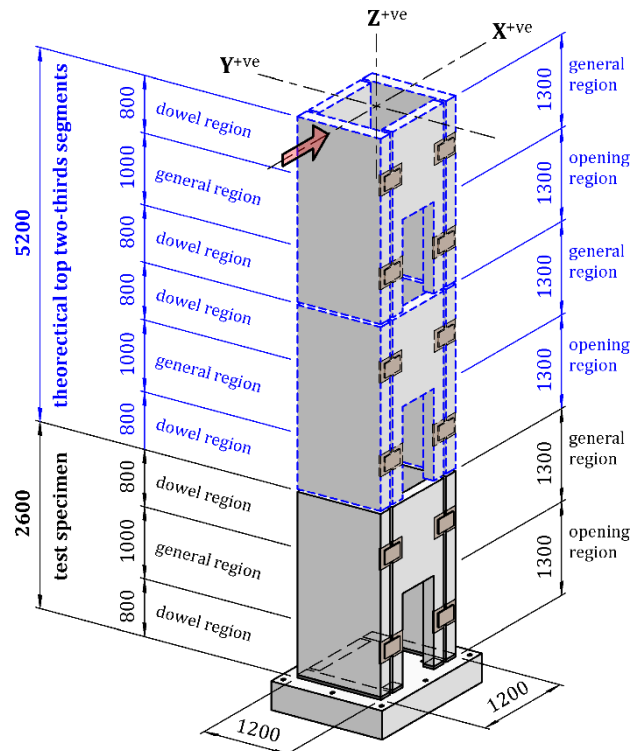


Fig. 8. Equivalent 1-DOF response.

The equivalent 1-DOF response for S05 was calculated using a novel approach developed by the authors. Wherein, the specimen itself, using the photogrammetry system, is used to determine empirical relationships that are then used to calculate a theoretical flexural and shear response of the top thirds of the specimen shown in Fig. 8. The effective displacement of the 1-DOF system is then equal to the measured displacement of the test specimen plus the flexural and shear contributions of the top two-thirds theoretical section of the core (i.e. Equation 1).

$$\Delta_{eff} = \Delta_{test} + \Delta_{t,f} + \Delta_{t,s} \quad (1)$$

Where: Δ_{test} is the displacement of the test specimen; $\Delta_{t,f}$ is the flexural displacement contribution from the top two thirds of the theoretical specimen; and $\Delta_{t,s}$ is the shear displacement contribution from the top two thirds of the theoretical specimen.

The empirical relationships in Fig. 9 were developed using the photogrammetry system and unpacking the different components of displacement for 16 discrete locations up the height of

specimen for eight different loading cycles. It was observed while developing the empirical relationships that the opening had little effect on the average moment-curvature response of the cross-section and similarly, the dowel region had little effect on the average shear modulus relationship. Therefore, only two empirical models were required for the curvature and shear modulus relationships, resulting in curvature-moment empirical relationships for dowel regions and general regions and effective shear modulus-moment relationships for regions with and without openings.

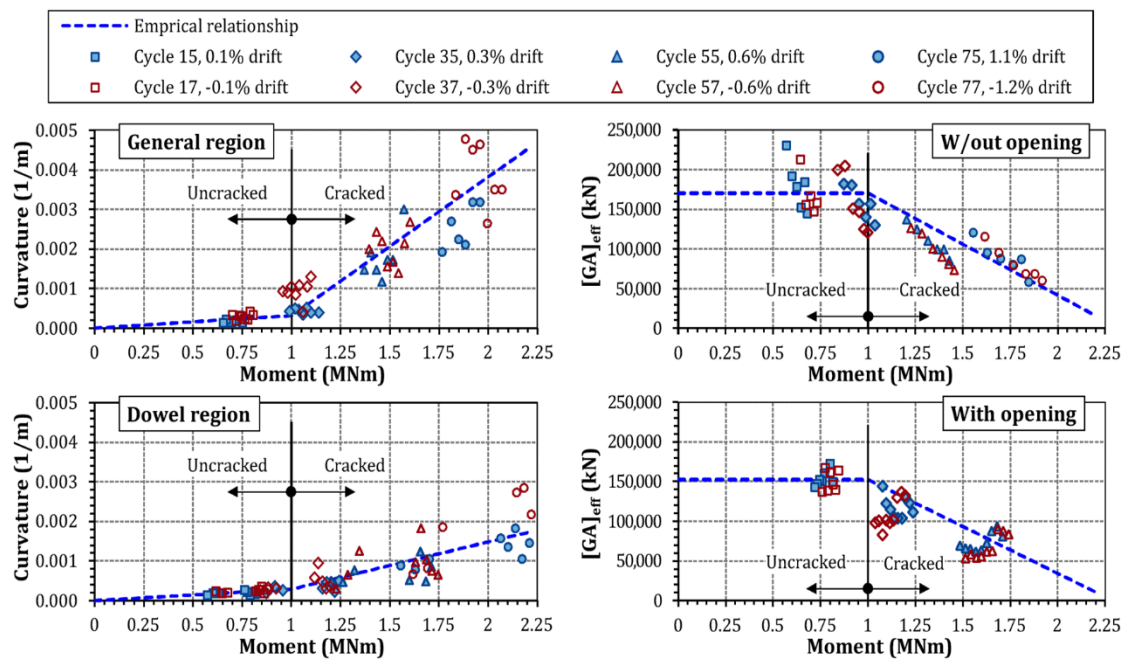


Fig. 9. Curvature-moment relationship for specimen S05.

To calculate both $\Delta_{t,f}$ and $\Delta_{t,s}$ the theoretical top two thirds was subdivided into 40 discrete segments. The curvature at each segment was calculated using the respective bending moment that would have been applied at that section and Fig. 9. This allowed a theoretical curvature distribution to be developed for the top two-thirds section of the core for each loading point of the test, which then could be double integrated to determine $\Delta_{t,f}$ for the top two-thirds.

Similarly, the shear displacement contribution from each segment was calculated using Equation 2, the respective bending moment that would have been applied at that section and Fig. 9. This then allowed $\Delta_{t,s}$ to be calculated by summing all the shear displacement contributions from each discrete segment in the theoretical top two-thirds of the core.

$$\Delta_{t,s,i} = \frac{FL_i}{[GA]_{eff}} \quad (2)$$

Where: $\Delta_{t,s,i}$ is the shear displacement contribution from the i -th segment; and L_i is the length of i -th discrete segment.

The force-displacement response of the 1-DOF system, determined using the procedure outlined above, for S05 is presented in Fig. 10. A bilinear response of 1-DOF response was constructed where the ‘up-branch’ is taken as a line that runs from the origin through the point corresponding to the first yield moment being reached. The first yield moment was taken as the theoretical moment when either the extreme tensile bar yields or compressive fibre reaches the concrete’s maximum compressive stress. The dowel reinforcement and vertical reinforcement in S05 is different, which means the yield moment and maximum moment capacity at the base of the wall and the top of the dowel connection will not be the same. It was found that the wall reinforcement above the dowel region was the critical section, which corresponded to the theoretical first yield moment occurring when a lateral load of 287 kN was applied. The ultimate displacement was taken as the point just before lateral load failure occurred, i.e. a 20% drop in lateral strength.

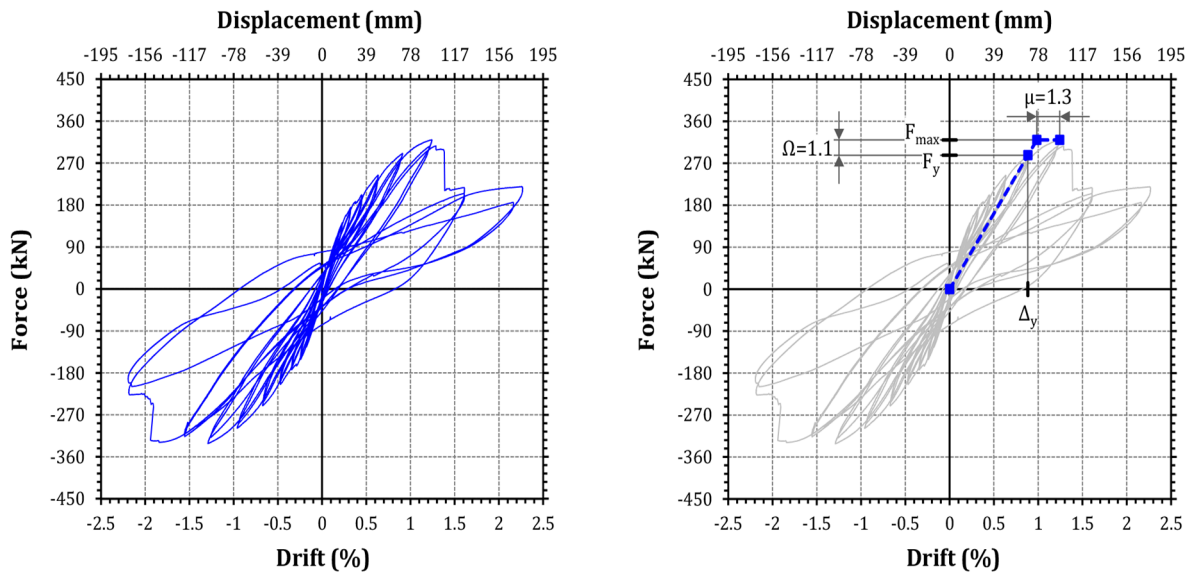


Fig. 10. Equivalent 1-DOF response of S05 (left) with bilinear approximation (right).

The effective stiffness (i.e. k_{eff}) of S05 is equal to the up-branch slope of the bilinear response shown Fig. 10 and the effective moment of inertia (i.e. I_{eff}) can be back calculated using the basic stiffness formula for a cantilever element, i.e. $k_{eff} = 3E_c I_{eff} / H_{eff}^3$. The average modulus of elasticity (i.e. E_c)

of the concrete used to construct S05 was calculated to be 33,100 MPa, which was determined using the equation from the Australian concrete code (i.e. AS 3600) and the average concrete compressive strength for the panels. The effective moment of inertia was therefore calculated to be 0.114 m⁴, which means the ratio of effective to gross moment of inertia of the section is 0.17.

This ratio of 0.17 for S05 was 25% lower than the equivalent ratio for the cast in-situ building core specimen, i.e. S02 (refer Menegon (2018)). This indicates precast building cores using WSP connections are somewhat more flexible than cast in-situ equivalents. This additional flexibility would very likely be proportionate to the stiffness of the WSP connection adopted. Further analytical studies are recommended.

The overstrength and displacement ductility of S05 was calculated to be 1.1 and 1.3 respectively (Fig. 10). These values are somewhat smaller than the values of 1.3 and 2.0, respectively, that the Australian concrete code (i.e. AS 3600 (Standards Australia, 2009)) and earthquake code (i.e. AS 1170.4 (Standards Australia, 2007)) typically allow for RC structures of this nature. The small displacement ductility is attributed to the low ductility reinforcement, while it is believed the smaller overstrength factor was due to the walls inability to develop 'full' composite action (as discussed in a following subsection), meaning the theoretical maximum moment capacity of the section could not be developed, hence reducing the amount of overstrength the wall could develop. The recently released 2018 version of AS 3600 (Standards Australia, 2018) has introduced new restrictions on the use of low ductility reinforcement in limited ductile RC walls following recommendations by the authors (Menegon et al., 2018).

3.5 Deformation Components

The different components of deformation for specimen S05 was determined using the contactless photogrammetry system. The flexure deformation was calculated by double-integrating the curvature distributions (i.e. Fig. 6) and the sliding shear deformations was determined directly from string potentiometers at the base of the wall. The shear deformation was then taken as the difference between the overall displacement and the combined flexural and sliding shear deformations.

It was found that flexural deformation accounted for 50% when the response of just the test specimen is consider; however, this value increases to 70% when assessed in relation to the equivalent 1-DOF

response calculated above. Marginal sliding shear deformation was observed during the test. The percentage of flexural deformation (i.e. 70%) was significantly less than the cast in-situ specimen (i.e. S02), which had a flexural deformation percentage of 90%. It is believed the large difference here is due to the fact the precast specimen was unable to develop full composite action.

3.6 Overall Composite Behaviour

It was shown in the previous sections that specimen S05 was more flexible than the similar cast in-situ building core specimen S02 tested previously by the authors, implying that the WSP connections were not stiff enough to allow full composite action to develop. This is confirmed by Fig. 12, which shows curvature profiles of specimen S05 for two positive and negative loading cycles. Curvature profiles are presented for a section of wall above the bottom stitch plates and at the base of the specimen, as shown in Fig. 11, and were calculated using the photogrammetry system.

It is shown in Fig. 12 that the maximum compressive and tensile strains in the web panel at the base of the S05 are greater than the compressive and tensile strains in the corresponding compressive and tensile flange panels of the building core. This can also be seen visually in Fig. 11, which shows the base of the web panel at load cycle 77 (i.e. -1.2% lateral drift), where the crack width at the tension end of the web panel is wider than the crack at the base of the tension flange. Additionally, spalling of the grout at the compression end of the web panel has occurred, while the base of the compression flange is fully intact without any spalling.

In a previous section it was shown that stitch plate #3 and #4 (refer Fig. 7) were close-to or on the verge of failing during load cycle 77 and 75 respectively. Despite this, it is clear that the WSP connections were not stiff enough to allow full composite action to developed, as Fig. 12(c) and Fig. 12(d) show that it was not able to be fully developed during load cycles 55 or 57 (i.e. $\pm 0.6\%$ lateral drift), during which the WSP were exhibiting an elastic response and the force in each connection did not exceed more than about 70% of its maximum capacity (refer Fig. 7).

The theoretical maximum bending moment capacity at the base of the wall (i.e. using the dowel bars as vertical reinforcement) and at the top of the dowels (i.e. using the panel bars as vertical reinforcement) was determined to be 3,025 kNm and 2,700 kNm respectively. It is noted these values are calculated using actual material properties for the section. This corresponds to lateral forces of

388 and 386 kN respectively (i.e. $3,025/7.8 = 388$ and $2,700/7.0 = 386$ kN respectively), inferring that the maximum lateral strength of S05 should have been approximately 386 kN. However, the maximum strength of S05, prior to the vertical reinforcement fracturing, was 302 and 314 kN in the positive and negative loading directions respectively. Meaning only 80% of the theoretical maximum moment capacity of the wall was able to be developed. This, in conjunction with curvature profiles in Fig. 12, show only partial composite action was developed in the cross-section.

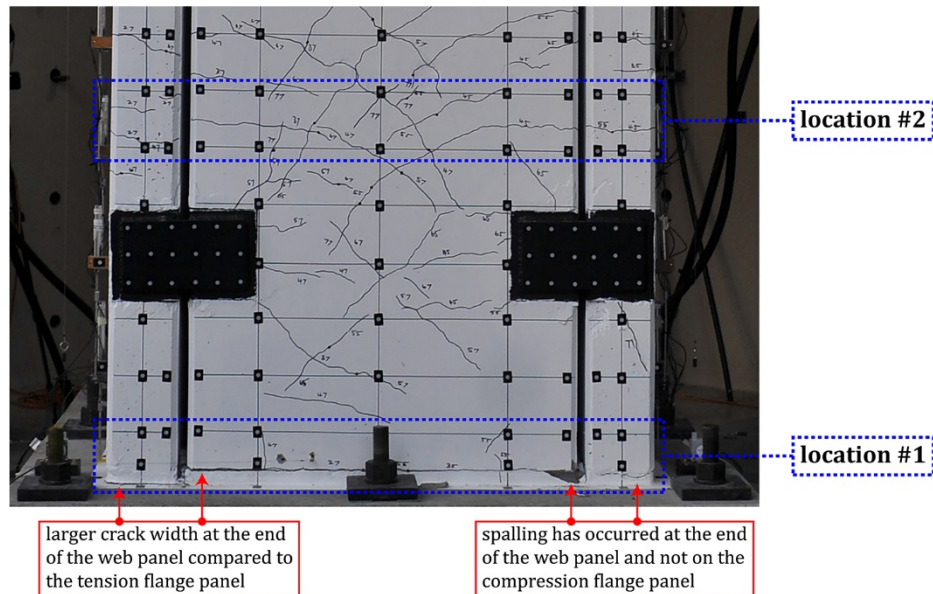


Fig. 11. Specimen S05, web panel elevation, load cycle 77, -1.2% lateral drift.

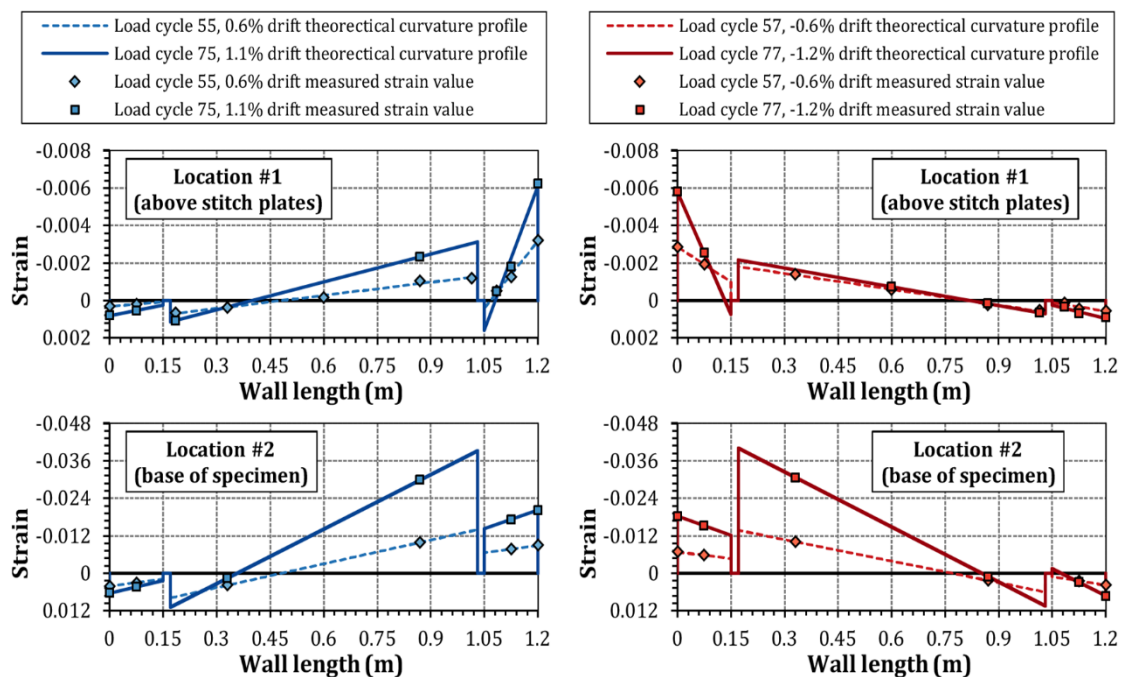


Fig. 12. Curvature profiles for specimen S05.

4 Summary and Concluding Remarks

This paper has provided an overview and detailed results analysis of the experimental testing of three largescale precast concrete building core specimens. The testing was undertaken to gain a better understanding of the in-plane lateral drift behaviour of precast core wall systems of this nature, which are widely used in low seismic regions, like Australia, yet have received littler research attention. The following recommendations and concluding remarks have been made:

1. Despite the lateral strength decreasing significantly, often below 20% of the maximum lateral capacity, the walls could withstand very large in-plane lateral drifts without axial load failure occurring (i.e. complete structural collapse). Specimens S03, S04 and S05 could withstand in-plane lateral drifts of 4.7%, 3.3% and 2.4% respectively before a 50% reduction in post-peak lateral capacity occurred. Further, with continued reduction in lateral capacity, the specimens were able to withstand in-plane lateral drifts of 6.5%, 8.0% and 4.9% respectively without axial load failure occurring, at which point the test was terminated.
2. Poor grouting at the base of the panels in specimens S03 and S04 resulted in stress concentrations and premature compression failures of the compression flange panel due to vertical tensile splitting. This would likely be mitigated by providing nominal cross ties at the top and bottom of the panel, which would mean the panel is then not relying on the concrete's tensile strength alone to prevent these potential tensile splitting failures, which may occur from accidental or unintended stress concentrations.
3. The WSP connections were not stiff enough to allow full composite action to be developed. This resulted in the ratio of effective to gross moment of inertia of specimen S05 being 0.17, which was 25% lower than a similar cast in-situ building core specimen tested previously by the authors. Further, this meant that only 80% of the theoretical maximum lateral capacity of S05 was developed before flexure failure occurred.
4. Specimens S03 and S04 had dowel bar reinforcement ratios less than the vertical reinforcement ratios in the respective panels above. This resulted in the development of one large crack at the base of the wall, with all the inelastic tensile strains concentrated at this single location. This allowed a rocking mechanism to develop, which then allowed for very large in-plane lateral drifts (i.e. >5%), without axial load failure of the wall occurring. This mechanism however, results in a

localised weak region at the base of the wall that would likely have little resistance to torsional actions since the cross-section at this location has developed large concentrated plastic tensile strains from the in-plane response. Torsional actions are common design actions for building cores in multi-storey buildings and therefore it is being recommended that this mechanism be avoided.

5. Specimen S05 showed that Low ductility reinforcement allows only marginal ductility to be developed before fracturing of the reinforcement occurs, which then results in a sudden reduction in lateral strength. While the core, immediately following the fracturing of the mesh, continued to have some residual capacity due to the web panel reinforcement and normal ductility perimeter bars, the overall integrity of the core was significantly compromised. Any torsional or lateral actions in the orthogonal direction applied at this point would have likely resulted in sudden failure or collapse.

5 Acknowledgements

The authors would like to thank the Brown family for their generous donation in establishing the Dr. William Piper Brown AM Scholarship, of which the lead author was the recipient.

6 Funding

This work was supported by the Australian Research Council (ARC) [grant number DP140103350, 2014].

7 Declaration of Interest

Declarations of interest: none.

8 References

- Almeida J, Prodan O, Rosso A, et al. (2017) Tests on Thin Reinforced Concrete Walls Subjected to In-plane and Out-of-plane Cyclic Loading. *Earthquake Spectra* 33: 323-345.
- American Concrete Institute. (2008) ACI ITG-5.1-07, Acceptance Criteria for Special Unbonded Post-Tensioned Precast Structural Walls Based on Validation Testing and Commentary. Farmington Hills, MI: American Concrete Institute.

- American Concrete Institute. (2013) ACI 374.2R-13 Guide for Testing Reinforced Concrete Structural Elements under Slowly Applied Simulated Seismic Loads. Farmington Hills, MI: American Concrete Institute.
- Dashti F, Dhakal RP and Pampanin S. (2017) Tests on slender ductile structural walls designed according to New Zealand Standard. *Bulletin of the New Zealand Society for Earthquake Engineering* 50: 504-516.
- Hashemi MJ, Al-Mahaidi R, Kalfat R, et al. (2015) Development and validation of multi-axis substructure testing system for full-scale experiments. *Australian Journal of Structural Engineering* 16: 302-315.
- Jiang H, Qiu H, Sun J, et al. (2019) Behavior of steel-concrete composite bolted connector in precast reinforced concrete shear wall. *Advances in Structural Engineering (in press)*.
- Lowes LN, Lehman DE, Birely AC, et al. (2012) Earthquake response of slender planar concrete walls with modern detailing. *Engineering Structures* 43: 31-47.
- Lu Y and Henry RS. (2017) Numerical modelling of reinforced concrete walls with minimum vertical reinforcement. *Engineering Structures* 143: 330-345.
- Lu Y, Henry RS, Gultom R, et al. (2017) Cyclic Testing of Reinforced Concrete Walls with Distributed Minimum Vertical Reinforcement. *Journal of Structural Engineering* 143.
- Menegon SJ. (2018) Displacement Behaviour of Reinforced Concrete Walls in Regions of Lower Seismicity. *Department of Civil and Construction Engineering*. Swinburne University of Technology.
- Menegon SJ, Wilson JL, Hughes S, et al. (2017a) Experimental testing of precast connections for jointed precast building cores. *Australian Earthquake Engineering Society 2017 Conference, November 24-26*. Canberra, ACT.
- Menegon SJ, Wilson JL, Lam NTK, et al. (2017b) Experimental testing of reinforced concrete walls in regions of lower seismicity. *Bulletin of the New Zealand Society for Earthquake Engineering* 50: 494-503.
- Menegon SJ, Wilson JL, Lam NTK, et al. (2017c) RC Walls in Australia: Reconnaissance Survey of Industry and Literature Review of Experimental Testing. *Australian Journal of Structural Engineering* 18: 24-40.
- Menegon SJ, Wilson JL, Lam NTK, et al. (2018) RC Walls in Australia: Seismic Design and Detailing to AS 1170.4 and AS 3600. *Australian Journal of Structural Engineering* 19: 67-84.
- Segura CL and Wallace JW. (2018) Seismic Performance Limitations and Detailing of Slender Reinforced Concrete Walls. *ACI Structural Journal* 115: 849-859.
- Seifi P, Henry RS and Ingham JM. (2016) Panel Connection Details in Existing New Zealand Precast Concrete Buildings. *Bulletin of the New Zealand Society for Earthquake Engineering* 49: 190-199.
- Seifi P, Henry RS and Ingham JM. (2019) In-plane cyclic testing of precast concrete wall panels with grouted metal duct base connections. *Engineering Structures* 184: 85-98.
- Shegay AV, Motter CJ, Elwood KJ, et al. (2018) Impact of Axial Load on the Seismic Response of Rectangular Walls. *Journal of Structural Engineering* 144.
- Standards Australia. (2007) AS 1170.4-2007 Structural design actions, Part 4: Earthquake actions in Australia. Sydney, NSW: Standards Australia.
- Standards Australia. (2009) AS 3600-2009 Concrete structures. Sydney, NSW: SAI Global Limited.
- Standards Australia. (2018) AS 3600:2018 Concrete structures. Sydney, NSW: Standards Australia Limited.
- Standards Australia and Standards New Zealand. (2001) AS/NZS 4671:2001 Steel reinforcing materials. Sydney and Wellington: Standards Australia International Ltd and Standards New Zealand.
- Sun J, Qiu H and Jiang H. (2018) Lateral load behaviour of a rectangular precast shear wall involving vertical bolted connections. *Advances in Structural Engineering* 22: 1211-1224.
- Sun J, Qiu H and Xu J. (2015) Experimental Verification of Vertical Joints in an Innovative Prefabricated Structural Wall System. *Advances in Structural Engineering* 18: 1071-1086.
- Wilson JL, Wibowo A, Lam NTK, et al. (2015) Drift Behaviour of Lightly Reinforced Concrete Columns and Structural Walls for Seismic Performance Assessment. *Australian Journal of Structural Engineering* 16: 62-74.